Emergence of Type-II Dirac Points in Graphynelike Photonic Lattices

Georgios G. Pyrialakos,[1] Nicholas S. Nye,[2] Nikolaos V. Kantartzis,[1] and Demetrios N. Christodoulides[2,*]
[1]School of Electrical and Computer Engineering, Aristotle University of Thessaloniki, Thessaloniki GR-54124, Greece
[2]College of Optics and Photonics, University of Central Florida, Orlando, Florida 32816-270, USA
(Received 13 May 2017; published 15 September 2017)

We theoretically demonstrate that a type-II class of tilted Dirac cones can emerge in generalized two-dimensional anisotropic lattice arrangements. This is achieved by introducing a special set of graphynelike exchange bonds by means of which the complete spectrum of the underlying Weyl Hamiltonian can be realized. Our *ab initio* calculations demonstrate a unique class of eigensolutions corresponding to a type-II class of Dirac fermionic excitations. Based on our approach, one can systematically synthesize a wide range of strongly anisotropic band diagrams having tilted Dirac cones with variable location and orientation. Moreover, we show that asymmetric conical diffraction, as well as edge states, can arise in these configurations. Our results can provide a versatile platform to observe, for the first time, optical transport around type-II Dirac points in two-dimensional optical settings under linear, nonlinear, and non-Hermitian conditions.

DOI: 10.1103/PhysRevLett.119.113901

The development of the relativistic Dirac equation incited intense activity along different directions, including, for example, the possibility for Dirac, Majorana, and Weyl fermions [1]. While for low energies (below the symmetry-breaking electroweak transition) the majority of fermions encountered in the standard model are of the Dirac type, the case is fundamentally different for neutrinos, whose nature still remains elusive. Weyl and Majorana particles have also been considered as viable candidates in interpreting parity-symmetry violations exhibited by neutrinos, when considered within the context of an extended standard model [2]. Recently, condensed matter settings and bosonic environments have provided viable alternatives for the study of such collective fermionic excitations.

The observation of massless Dirac fermions in graphene systems [3] was instrumental in instigating similar explorations in other fields beyond solid state physics [4–8], like, for example, photonics and ultracold atoms [9–14]. Quite lately, there has been a resurgence of interest in generalized forms of the so-called Weyl Hamiltonian, which also involves the identity σ_0 matrix, responsible for tilting the Weyl cones. Based on these generalizations, one can identify two distinct classes of Weyl points (WPs): (i) type I with pointlike Fermi surfaces and (ii) type II with conical-like Fermi surfaces. While type-I WPs can be encountered in various arrangements [15–19], there are ongoing efforts, both experimental and theoretical, to explore the prospect of type-II Weyl-like features in lattices [20–25]. In this respect, the Lorentz-violating type-II Weyl quasiparticles, whose existence is impossible in particle physics due to the Lorentz-covariant nature of the standard model, are associated with the resulting strongly tilted Weyl cones. Since condensed matter [20–22] and bosonic arrangements (atomic, photonic, etc.) [23–25] are not subject to such constraints, both can provide a fertile ground for exploring different aspects of type-II WPs.

The question now arises as to whether a similar classification can be made for Dirac points (DPs). While type-I Dirac cones (DCs) are common in honeycomb configurations and other two- (2D) and three-dimensional (3D) materials [3–14], this is not the case for type-II DCs. In recent studies, type-II Dirac semimetals [26–29] and 3D topological photonic crystal structures [30] have been demonstrated. Along these lines, of interest would be to identify 2D photonic systems with analogous dispersion characteristics, akin to those proposed in solid state physics [31,32]. In this respect, one can experimentally explore a number of possibilities, including photonic Landau levels [12,13], *Zitterbewugung* [33], and Klein tunneling [34], in highly anisotropic environments.

In this Letter, we investigate, for the first time, an all-dielectric noncentrosymmetric photonic-lattice realization, whose band structure exhibits 2D type-II DPs. By mimicking the molecular bonds in an artificial carbon allotrope (graphyne [35]), we propose a variant of a centered-square lattice having adjustable waveguide chains between adjacent sites. In this manner, the dispersion diagrams of this lattice can transition from type-I to type-II DCs, by gradually ordering the exchange bonds involved in the generalized Weyl Hamiltonian. Based on *ab initio* calculations, we have developed a systematic methodology, through which one can at will control the orientation and position of the ensued highly anisotropic DCs. Furthermore, we demonstrate the existence of edge states in ribbon geometries, and we show that asymmetric conical diffraction can take place, by exciting the graphynelike lattice near the type-II DP. The degrees of freedom offered by our structure, along with the ability to fine-tune its design parameters via existing high-precision laser -writing techniques [36], can enable further the understanding of the underlying transport mechanisms associated with these

exotic quasiparticles under linear, nonlinear, and non-Hermitian conditions [37–40].

We begin our theoretical analysis by considering the generalized Weyl Hamiltonian in an SU(2) space, as spanned by the Pauli matrices. In this representation, near a singular DP, the Hamiltonian can be effectively expressed as

$$H = \sum_{n=0}^{2} \mathbf{u}_n \cdot \mathbf{k}\sigma^n, \tag{1}$$

where $\mathbf{u}_n = (u_n^x, u_n^y)$ is the velocity vector, $\mathbf{k} = (k_x, k_y)$ is the transverse wave vector, σ^0 is the unitary matrix, and σ^n, for $n = 1, 2$, are the first two Pauli matrices. By employing an appropriate transformation [7], Eq. (1) can assume the form of the minimal Weyl Hamiltonian $H = v_0^x k_x \sigma^0 + v_0^y k_y \sigma^0 + v_1^x k_x \sigma^1 + v_2^y k_y \sigma^2$, where $v_{0/1}^{x/y}$ now represent effective velocity terms. The case of isotropic Dirac cones in graphene lattices can be simply retrieved, when $v_0^x = v_0^y = 0$ [Fig. 1(a)]. On the other hand, anisotropic or tilted DCs can emerge only provided that $v_x^0 \neq 0$ or $v_y^0 \neq 0$. As these coefficients increase in size, the resulting tilt becomes even stronger. The critical condition $(v_0^x/v_1^x)^2 + (v_0^y/v_2^y)^2 > 1$ marks the onset of type-II Dirac points [Fig. 1(b)]. In this regime, the photonic band diagram can become sufficiently anisotropic, so tipping of the cones can take place. As an upshot, the intersection of the upper and lower photonic bands with the $\beta = 0$ plane (Fermi level) leads to hyperbolic curves. Moreover, within the same band, the group velocity or gradient of the propagation constant β does not change sign at the singularity point. These represent unique signatures of type-II DPs [41], that are otherwise absent in conventional type-I DPs.

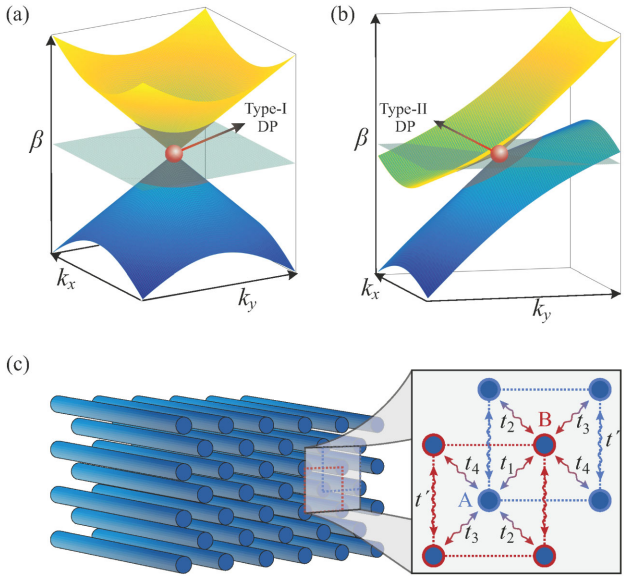

FIG. 1. Dispersion band diagrams near the DPs for: (a) type-I DCs with a pointlike Fermi surface and (b) type-II DCs with a conical-like Fermi surface. (c) The centered-square lattice is shown in 3D (left), while the constituent A (blue) and B (red) square sublattices, along with their inter- and intracouplings (t_1, t_2, t_3, t_4, t'), are depicted in a magnified 2D view (right).

In order to investigate the complete Weyl Hamiltonian spectrum, we first consider a centered-square lattice, as shown in Fig. 1(c). Every site consists of a single-mode waveguide element that is evanescently coupled to its neighbors. Based on tight binding considerations, one can then introduce auxiliary diagonal terms in the Hamiltonian of the system, that can account for beyond-nearest-neighbor interactions via the hopping term t'. Here, we will study the most general case, where the nearest-neighbor interactions are unequal $(t_1 \neq t_2 \neq t_3 \neq t_4)$. Under these assumptions, this generalized arrangement can be considered as a superposition of two displaced square sublattices A and B [Fig. 1(c)], whose coupled evolution equations can be described via

$$i\partial_z \varphi_{A_{m,n}} = \sum_{\substack{p=0,1\\q=0,1}} t_{(pq)} \varphi_{B_{m-p,n-q}} + t' \sum_{q=-1,1} \varphi_{A_{m,n+q}}, \tag{2a}$$

$$i\partial_z \varphi_{B_{m,n}} = \sum_{\substack{p=0,1\\q=0,1}} t_{(pq)} \varphi_{A_{m+p,n+q}} + t' \sum_{q=-1,1} \varphi_{B_{m,n+q}}, \tag{2b}$$

where φ_A and φ_B represent optical field modal amplitudes at site (m, n) and $t_{(pq)}$ the coupling coefficients between sublattices A and B, respectively.

The Floquet-Bloch solutions of Eqs. (2) can be directly obtained from the effective Hamiltonian

$$H_{\mathbf{k}} = \begin{pmatrix} \tilde{h}(\mathbf{k}) & h^*(\mathbf{k}) \\ h(\mathbf{k}) & \tilde{h}(\mathbf{k}) \end{pmatrix},$$

with $h(\mathbf{k}) = (t_1 + t_3)\cos K_1 + (t_2 + t_4)\cos K_2 + i[(t_1 - t_3)\sin K_1 - (t_2 - t_4)\sin K_2]$, $\tilde{h}(\mathbf{k}) = 2t'\cos k_y$, $K_1 = (k_x + k_y)/2$, and $K_2 = (k_x - k_y)/2$. Moreover, the emergence of DCs requires the coalescence of the eigenvalues of H at the singularity, which is satisfied iff $|h(\mathbf{k})| = 0$. This implies for the location $\mathbf{k}^{\mathrm{DP}} = (k_x^{\mathrm{DP}}, k_y^{\mathrm{DP}})$ of the Dirac points that

$$k_x^{\mathrm{DP}} = 2\tan^{-1}\sqrt{-\frac{(t_3 + t_4)^2 - (t_1 + t_2)^2}{(t_3 - t_4)^2 - (t_1 - t_2)^2}}, \tag{3a}$$

$$k_y^{\mathrm{DP}} = 2\tan^{-1}\sqrt{-\frac{(t_3 + t_2)^2 - (t_1 + t_4)^2}{(t_3 - t_2)^2 - (t_1 - t_4)^2}}. \tag{3b}$$

In this respect, the velocity terms appearing in Eq. (1) are given by $u_0^x = \partial\tilde{h}(\mathbf{k})/\partial k_x$, $u_0^y = \partial\tilde{h}(\mathbf{k})/\partial k_y$, $u_1^x = \partial \mathrm{Re}\{h(\mathbf{k})\}/\partial k_x$, $u_1^y = \partial \mathrm{Re}\{h(\mathbf{k})\}/\partial k_y$, $u_2^x = \partial \mathrm{Im}\{h(\mathbf{k})\}/\partial k_x$, and $u_2^y = \partial \mathrm{Im}\{h(\mathbf{k})\}/\partial k_y$. Additionally, the gradient of the dispersion relation $\mathbf{w} = (w_x, w_y) = \partial\beta(\mathbf{k})/\partial\mathbf{k}$ can be acquired from $w_x = \pm\partial(|h(\mathbf{k})|)/\partial k_x$ and $w_y = \partial[\tilde{h}(\mathbf{k}) \pm |h(\mathbf{k})|]/\partial k_y$. In this configuration, the factor

$\partial\tilde{h}(\mathbf{k})/\partial k_y$ is responsible for the tilt of the DCs along the y direction. Based on the previous results, it is clear that the induced tilt depends solely on the hopping term t', while the position and slope of the cones are only functions of the couplings t_1, t_2, t_3, and t_4.

Both velocities (u_0^x, u_0^y) appear effectively as primary diagonal terms in the Hamiltonian matrix. Because of their linear dependence on the wave number $\mathbf{k}$, they cannot lead to a gap, since the corresponding terms in the Hamiltonian attain a zero value at the degenerate Dirac point. This behavior is quite different from that encountered in deformed honeycomb configurations with constant diagonal detuning terms [37], where Dirac cones can be sustained only if non-Hermitian gain and loss elements are also employed. In our system, instead, gapless states can be retained, while at the same time strongly tilted type-II DCs can be introduced. What makes this possible is the high degree of flexibility offered by the five design parameters (t_1, t_2, t_3, t_4, t'). The only restriction arises from the fact that these parameters must be chosen in such a way that wave vector components $(k_x^{\mathrm{DP}}, k_y^{\mathrm{DP}})$ are real. Note that, in the isotropic case $(t_1 = t_2 = t_3 = t_4)$, Eqs. (3) exhibit a singularity. Thus, perturbations around this point can lead to a topological creation or destruction of the DCs.

Based on these considerations, we then synthesize the proposed lattice model. To do so, the nearest-neighbor hopping terms must be unequal, while the next-nearest-neighbor coupling strength t' is enhanced, in order to produce highly anisotropic DCs. In this work, both aspects are simultaneously addressed by incorporating waveguide chains that play a role akin to that of exchange bonds among the molecular units of graphyne. Here, the sites of the original configuration [Fig. 1(c)] are referred to as the *main lattice sites* (belonging to sublattices A and B) so as to distinguish them from the additional waveguide (chain) elements, which will be subsequently introduced.

To examine the properties of such chains, we herein assume, for simplicity, four cores arranged in a one-dimensional (1D) mirror-symmetric formation, as shown in Fig. 2(a). In this configuration, the modal field amplitudes φ_i satisfy

$$\beta\varphi_{-2} = V_2\varphi_{-2} + t_{12}\varphi_{-1}, \tag{4a}$$

$$\beta\varphi_{-1} = V_1\varphi_{-1} + t_{12}\varphi_{-2} + t_{11}\varphi_1, \tag{4b}$$

$$\beta\varphi_1 = V_1\varphi_1 + t_{11}\varphi_{-1} + t_{12}\varphi_2, \tag{4c}$$

$$\beta\varphi_2 = V_2\varphi_2 + t_{12}\varphi_1, \tag{4d}$$

where V_1 and V_2 represent on-site optical potential terms. Given the underlying mirror-inversion symmetry exhibited by this chain [Fig. 2(a)], one can find that, around the singularity point $(\beta \approx 0)$, Eqs. (4) are effectively reduced to

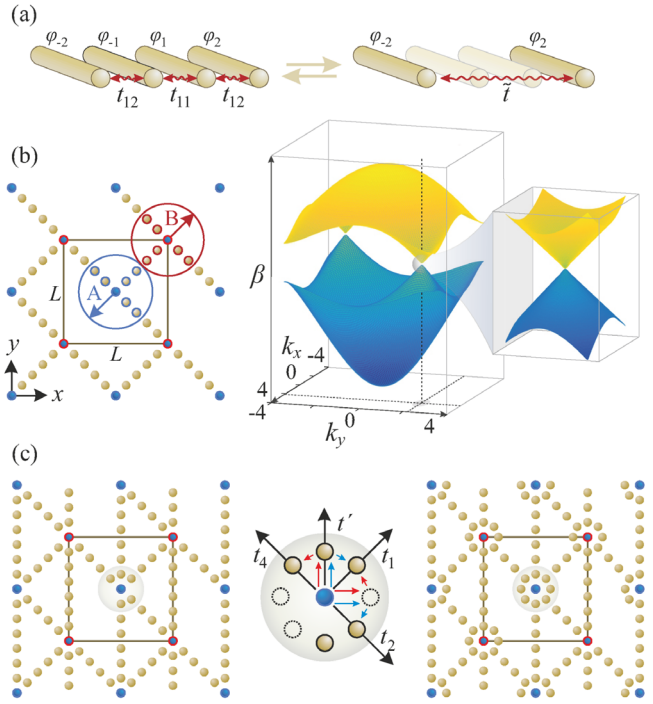

FIG. 2. (a) 1D chain of waveguides (left) and equivalent model (right), consisting now of only the two edge waveguide cores coupled via an effective hopping parameter $\tilde{t}$. (b) The centered-square lattice, after the inclusion of the main waveguide chains, is shown on the left. The corresponding dispersion diagram, together with a magnified view of the linear dispersion in the vicinity of a degenerate type-I DP, is shown on the right. (c) The lattice after incorporating the secondary waveguide chains along the y direction (left panel). For the mitigation of undesired effects, stemming from the asymmetric couplings between adjacent waveguide chains, we slightly alter the geometry (middle panel) to locally attain a more symmetric topology in the vicinity of the main lattice points, as depicted on the right.

$$\beta\varphi_2 = \left(V_2 - \frac{t_{12}V_1}{V_1^2 - t_{11}^2}\right)\varphi_2 + \frac{t_{12}^2 t_{11}}{V_1^2 - t_{11}^2}\varphi_{-2}, \tag{5a}$$

$$\beta\varphi_{-2} = \frac{t_{12}^2 t_{11}}{V_1^2 - t_{11}^2}\varphi_2 + \left(V_2 - \frac{t_{12}V_1}{V_1^2 - t_{11}^2}\right)\varphi_{-2}. \tag{5b}$$

In other words, Eqs. (5) provide an alternative description of the system, since the action of the two central cores in the chain can be essentially described by an effective hopping parameter $\tilde{t} = t_{12}^2 t_{11}/(V_1^2 - t_{11}^2)$, as shown in Fig. 2(a). Without any loss of generality, we can extend this same concept in similar arrangements involving more waveguide elements. Furthermore, by locally perturbing a waveguide anywhere in the 1D lattice (e.g., by slightly changing its refractive index), we can increase or decrease this effective hopping term $\tilde{t}$. This flexibility allows for the realization of generalized Weyl Hamiltonians near a degenerate point.

An example of such a lattice topology, supporting isotropic type-I DPs, is shown in Fig. 2(b). In addition to the unit cell of Fig. 1(c), three *main waveguide chains*

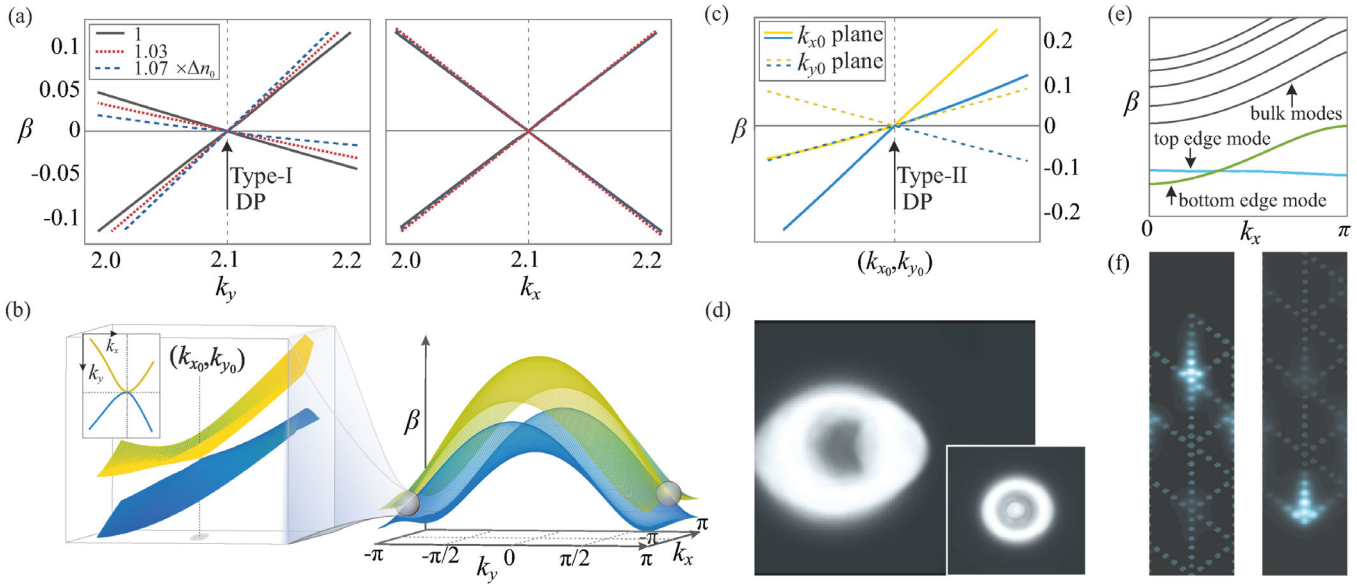

FIG. 3. Dispersion curves (type-I DP) along $k_x = 2\pi/3$ (left) and $k_y = 2\pi/3$ (right), corresponding to the noncentrosymmetric graphynelike arrangement, depicted in the right panel in Fig. 2(c). Each graph is related to a different value of the refractive index difference of the secondary chains ($\Delta n_{\mathrm{SC}} = 1, 1.03, 1.07 \times \Delta n_0$). In all cases, the refractive index of the main chains is kept identical to that of the main lattice nodes ($\Delta n_{\mathrm{MC}} = \Delta n_0 = 0.002$). By increasing the value of Δn_{SC}, this tilt becomes pronounced enough that tipping of the cones takes place (type-II DCs). This becomes evident for $\Delta n_{\mathrm{SC}} = 1.3\Delta n_0$ in (b), which depicts the respective bulk band structure throughout the Brillouin zone (right), along with a magnified view of the type-II DPs (left, inset: hyperboliclike intersection with the $\beta = 0$ plane). The linear dispersion near the Dirac point, located at $(k_{x_0}, k_{y_0}) = (2\pi/3, 2\pi/3)$, is shown in (c). In (d), asymmetric and symmetric conical diffraction (inset) is demonstrated, after exciting (near the generate point) the lattices of Figs. 2(c) ($\Delta n_{\mathrm{SC}} = 1.3\Delta n_0$) and 2(b) ($\Delta n_{\mathrm{SC}} = 0$), respectively. In (e) and (f), the band diagram and respective eigenmode distribution are depicted for top (left) and bottom (right) ribbonlike edge states, supported by the lattice in the right panel in Fig. 2(c) for $\Delta n_{\mathrm{SC}} = 1.3\Delta n_0$.

(MCs) have been inserted between nearest-neighbor sites in such a way so as to satisfy the relations $t_1 = t_2 = t_4$ and $t_3 = t' \approx 0$ (thus inducing a P-symmetry breaking). For this set of parameters, Eqs. (3) admit real solutions, and hence isotropic DCs emerge at the wave vector locations $\mathbf{k}_1^{\mathrm{DP}} = (2\pi/3, 2\pi/3)$ and $\mathbf{k}_2^{\mathrm{DP}} = (-2\pi/3, -2\pi/3)$. Subsequently, the optical band structure can be retrieved by numerically solving the paraxial wave equation (Floquet-Bloch solutions) for this unit cell. Our results are in excellent agreement with those obtained from the tight-binding approximation, as shown in Fig. 2(b). In this same figure, the upper and lower photonic bands correspond to the lowest-order modes (even and odd), with respect to the nodes of sublattices A and B. To implement this configuration, we use the following physical parameters: The diameter and refractive index of the waveguides (for both the main lattice points and the MCs) are set to be $D = 6$ μm and $n = n_{\mathrm{MC}} = 1.452$, respectively, while the refractive index of the background medium is $n_b = 1.45$ ($\Delta n_0 = \Delta n_{\mathrm{MC}} = 0.002$) at a wavelength of $\lambda = 1550$ nm. Such values can be readily attained experimentally via laser-writing techniques [36] or optothermal nonlinearities [42].

In what follows, we introduce anisotropicity in the photonic band diagram by means of *secondary waveguide chains* (SCs) between next-nearest-neighbor sites, as shown in Fig. 2(c). To identify where the transition from a type-I to type-II DP will occur, we numerically investigate different cases [Figs. 3(a)–3(d)], where we progressively increase the refractive index difference Δn_{SC} of the secondary chain waveguides while keeping the remaining parameters the same. In Fig. 3(a), the Dirac point is of type I, as long as $\Delta n_{\mathrm{SC}} \leq 1.07\Delta n_0$. Once Δn_{SC} exceeds these values, a strongly tilted DC emerges [Figs. 3(b) and 3(c)]. In this case, the intersection of the upper and lower photonic bands with the $\beta = 0$ plane leads to hyperbolic-like contours (open "Fermi" surfaces), which is a characteristic signature of type-II DPs.

To gain insight into the underlying transport processes, we simulate the optical beam dynamics in a lattice, consisting of 2500 unit cells. A Gaussian beam is used to probe these effects near the degenerate DP. When the Dirac cones are strongly tilted, we numerically observe a light ring, which now constantly drifts along the direction predicted by the slope of the respective asymmetric band diagram in the vicinity of a type-II singularity [Fig. 3(d)]. On the other hand, isotropic propagation is expected [11], when the secondary chains are excluded [inset in Fig. 3(d)].

Given its nontrivial topology, of interest would be to study the characteristics of edge states, supported by this generalized centered-square lattice. Along these lines, we truncate this arrangement laterally in the y direction (ribbonlike structure), and, subsequently, we obtain the band spectrum

as a function of k_x. As shown in Fig. 3(e), two distinct classes of modes emerge: (i) bulk modes [arising from the bulk band structure of Fig. 3(b)] and (ii) edge modes [existing at the edges—Fig. 3(f)]. The inherent anisotropy of the lattice, along with the different edge topologies, leads to nonstationary counterpropagating edge states. Their respective intersection in the band diagram is dictated by the strength of the graphynelike exchange bonds. Note that the time-invariant nature of the proposed model indicates that the nonchiral edge states cannot be protected against random backscattering defects [17]. This latter feature can be introduced, provided the waveguide elements are appropriately modulated along the propagation direction [25,43].

In conclusion, in the present Letter we have theoretically provided the necessary conditions for the emergence of type-II Dirac cones in a noncentrosymmetric version of the centered-square photonic lattice with graphynelike exchange bonds. By doing so, we demonstrated that the photonic dispersion diagram can be modified at will, thus allowing control over the orientation, location, and anisotropy of the emerging DCs. Also, effects like asymmetric conical diffraction and edge states in ribbonlike structures have been shown to exist near the type-II point of degeneracy. The proposed configurations can be used to investigate exceptional point dynamics in the vicinity of type-II DPs in non-Hermitian and PT-symmetric systems. This class of massless type-II Dirac fermions may also lead to novel topologically nontrivial architectures and might pave the way to explore complex light behavior in highly anisotropic dispersion environments.

This work was supported by the National Science Foundation (NSF) (Grant No. DMR-1420620) and Qatar National Research Fund (QNRF) (Grant No. 9-020-1-006). N. S. N. acknowledges the support of the Alexander S. Onassis Public Benefit Foundation and the Foundation for Education and European Culture.

*Corresponding author.
demetri@creol.ufc.edu

[1] P. B. Pal, Am. J. Phys. **79**, 485 (2011).
[2] D. Colladay and V. A. Kostelecký, Phys. Rev. D **58**, 116002 (1998).
[3] K. S. Novoselov, A. K. Geim, S. V. Morozov, D. Jiang, M. I. Katsnelson, I. V. Grigorieva, S. V. Dubonos, and A. A. Firsov, Nature (London) **438**, 197 (2005).
[4] X. Wan, A. M. Turner, A. Vishwanath, and S. Y. Savrasov, Phys. Rev. B **83**, 205101 (2011).
[5] S. M. Young, S. Zaheer, J. C. Y. Teo, C. L. Kane, E. J. Mele, and A. M. Rappe, Phys. Rev. Lett. **108**, 140405 (2012).
[6] A. Kobayashi, S. Katayama, Y. Suzumura, and H. Fukuyama, J. Phys. Soc. Jpn. **76**, 034711 (2007).
[7] M. O. Goerbig, J.-N. Fuchs, G. Montambaux, and F. Piéchon, Phys. Rev. B **78**, 045415 (2008).
[8] Z. Wang, X.-F. Zhou, X. Zhang, Q. Zhu, H. Dong, M. Zhao, and A. R. Oganov, Nano Lett. **15**, 6182 (2015).
[9] Z. Wang, Y. D. Chong, J. D. Joannopoulos, and M. Soljačić, Phys. Rev. Lett. **100**, 013905 (2008).
[10] X. Huang, Y. Lai, Z.-H. Hang, H. Zheng, and C. T. Chan, Nat. Mater. **10**, 582 (2011).
[11] O. Peleg, G. Bartal, B. Freedman, O. Manela, M. Segev, and D. N. Christodoulides, Phys. Rev. Lett. **98**, 103901 (2007).
[12] M. C. Rechtsman, J. M. Zeuner, A. Tünnermann, S. Nolte, M. Segev, and A. Szameit, Nat. Photonics **7**, 153 (2013).
[13] H. Schomerus and N. Y. Halpern, Phys. Rev. Lett. **110**, 013903 (2013).
[14] S.-L. Zhu, B. Wang, and L.-M. Duan, Phys. Rev. Lett. **98**, 260402 (2007).
[15] A. A. Burkov and L. Balents, Phys. Rev. Lett. **107**, 127205 (2011).
[16] H. Miyake, G. A. Siviloglou, C. J. Kennedy, W. C. Burton, and W. Ketterle, Phys. Rev. Lett. **111**, 185302 (2013).
[17] L. Lu, J. D. Joannopoulos, and M. Soljačić, Nat. Photonics **8**, 821 (2014).
[18] S. Y. Xu, I. Belopolski, N. Alidoust, M. Neupane, G. Bian, C. Zhang, R. Sankar, G. Chang, Z. Yuan, C. C. Lee, and S. M. Huang, Science **349**, 613 (2015).
[19] L. Lu, Z. Wang, D. Ye, L. Ran, L. Fu, J. D. Joannopoulos, and M. Soljačić, Science **349**, 622 (2015).
[20] A. A. Soluyanov, D. Gresch, Z. Wang, Q. Wu, M. Troyer, X. Dai, and B. A. Bernevig, Nature (London) **527**, 495 (2015).
[21] K. Deng, G. Wan, P. Deng, K. Zhang, S. Ding, E. Wang, M. Yan, H. Huang, H. Zhang, Z. Xu, and J. Denlinger, Nat. Phys. **12**, 1105 (2016).
[22] G. Autes, D. Gresch, M. Troyer, A. A. Soluyanov, and O. V. Yazyev, Phys. Rev. Lett. **117**, 066402 (2016).
[23] Y. Xu, F. Zhang, and C. Zhang, Phys. Rev. Lett. **115**, 265304 (2015).
[24] W. J. Chen, M. Xiao, and C. T. Chan, Nat. Commun. **7**, 13038 (2016).
[25] J. Noh, S. Huang, D. Leykam, Y. D. Chong, K. Chen, and M. C. Rechtsman, Nat. Phys. **13**, 611 (2017).
[26] H. Huang, S. Zhou, and W. Duan, Phys. Rev. B **94**, 121117 (2016).
[27] C. Le, S. Qin, X. Wu, X. Dai, P. Fu, and J. Hu, arXiv:1606.05042.
[28] T. R. Chang, S. Y. Xu, D. S. Sanchez, S. M. Huang, G. Chang, C. H. Hsu, G. Bian, I. Belopolski, Z. M. Yu, X. Xu, and C. Xiang, arXiv:1606.07555.
[29] P. J. Guo, H. C. Yang, K. Liu, and Z. Y. Lu, Phys. Rev. B **95**, 155112 (2017).
[30] H. X. Wang, Y. Chen, Z. H. Hang, H. Y. Kee, and J. H. Jiang, arXiv:1703.09899.
[31] L. Muechler, A. Alexandradinata, T. Neupert, and R. Car, Phys. Rev. X **6**, 041069 (2016).
[32] H. Zhang, Y. Xie, C. Zhong, Z. Zhang, and Y. Chen, arXiv:1612.08456.
[33] X. Zhang, Phys. Rev. Lett. **100**, 113903 (2008).
[34] F. Dreisow, R. Keil, A. Tünnermann, S. Nolte, S. Longhi, and A. Szameit, Europhys. Lett. **97**, 10008 (2012).

[35] D. Malko, C. Neiss, F. Viñes, and A. Görling, Phys. Rev. Lett. **108**, 086804 (2012).
[36] A. Szameit and S. Nolte, J. Phys. B **43**, 163001 (2010).
[37] A. Szameit, M. C. Rechtsman, O. Bahat-Treidel, and M. Segev, Phys. Rev. A **84**, 021806(R) (2011).
[38] E. M. Graefe and H. F. Jones, Phys. Rev. A **84**, 013818 (2011).
[39] H. Ramezani, T. Kottos, V. Kovanis, and D. N. Christodoulides, Phys. Rev. A **85**, 013818 (2012).
[40] B. Zhen, C. W. Hsu, Y. Igarashi, L. Lu, I. Kaminer, A. Pick, S. L. Chua, J. D. Joannopoulos, and M. Soljačić, Nature (London) **525**, 354 (2015).
[41] M. Trescher, B. Sbierski, P. W. Brouwer, and E. J. Bergholtz, Phys. Rev. B **91**, 115135 (2015).
[42] S. Shabahang, N. S. Nye, C. Markos, D. N. Christodoulides, and A. F. Abouraddy, Opt. Lett. **42**, 1919 (2017).
[43] M. C. Rechtsman, J. M. Zeuner, Y. Plotnik, Y. Lumer, D. Podolsky, F. Dreisow, S. Nolte, M. Segev, and A. Szameit, Nature (London) **496**, 196 (2013).